OPEN

NPG Asia Materials (2016) 8, e335; doi:10.1038/am.2016.184
www.nature.com/am

ORIGINAL ARTICLE

The pH-switchable agglomeration and dispersion behavior of fluorescent Ag nanoclusters and its applications in urea and glucose biosensing

Jiang Xue Dong[1], Zhong Feng Gao[1], Ying Zhang[1,2], Bang Lin Li[1], Wei Zhang[3], Jing Lei Lei[4], Nian Bing Li[1] and Hong Qun Luo[1]

Water-soluble fluorescent Ag nanoclusters (Ag NCs) with distinct pH-switchable agglomeration and spectral signal responses are prepared using a facile etching method. Increased and decreased pH cause the Ag NCs to switch between agglomeration and dispersion, accompanied by decreases in and recoveries of fluorescence intensity and absorbance. The pH switchable behavior of the Ag NCs is attributed to carboxyl groups on the nanocluster surface that are rich in the citrate and amido functional groups of ligands (glutathione), creating an easily formed, weak molecular interaction among Ag NCs (for example, hydrogen bonding) and maintaining a balance in the colloidal solution, whereas a change in pH will disrupt the balance, leading to the reversible agglomeration of Ag NCs and the switchable spectral signal response. In addition, because urea and glucose can change the pH of a solution by producing NH_3 and gluconic acid in enzyme-catalyzed reactions, the pH-switchable behavior of the Ag NCs is used to develop them as an optical probe to establish a regenerated biosensing platform for the sensitive and selective detection of urea and glucose, and the test results are satisfactory.
NPG Asia Materials (2016) **8,** e335; doi:10.1038/am.2016.184; published online 9 December 2016

INTRODUCTION

Metal nanoparticles on an ~2 nm scale are defined as metal nanoclusters, and they show physicochemical properties that are significantly different from those of their bulk form. Fluorescent metal nanoclusters composed of a small number of atoms have attracted research interest because of their unique properties and molecule-like behavior.[1,2] In recent decades, many fluorescent metal nanoclusters, especially nanoclusters of Au and Ag, among noble metals, have been reported, and the ligands that stabilize these small nanoparticles have a key role in their fundamental properties: (i) ligands can influence optical properties by transferring their charge to the metal cores or by directly donating delocalized electrons contained on them to the metal cores;[3,4] (ii) surface ligands can determine the physical properties of nanoclusters (for example, hydrophily and hydrophoby), and amphiphilic metal nanoclusters can be produced by skillfully controlling the type and amount of ligands;[5] (iii) the functional groups of the surface ligands determine the chemical properties of the metal nanoclusters; thus, fluorescent nanoclusters can be more widely used as probes for detecting various targets.[6,7] Moreover, published studies show that the optical properties of Au and Ag nanoclusters (Ag NCs) protected by thiols are more likely to be dependent on the ligands and functional groups on the nanocluster surface,[8] and because of good biocompatibility and active chelation to metal atoms, glutathione (GSH) has been widely used as a stabilizer to obtain fluorescent Au and Ag NCs for use in the biomedicine and biosensor fields.[9–11] In addition, etching colloidal metal nanocrystals with ligands containing certain functional groups is a recognized classical route to obtain fluorescent metal nanoclusters,[12] and etching processes using thiol to obtain Au and Ag NCs have been developed in many laboratories. However, the reported etching methods to obtain Au and Ag NCs always involve toxic organic solvents, rigorous reaction conditions (for example, oxygen-free and high temperature) and complicated procedures.[13–15]

Among numerous studies on metal nanoclusters, the aggregation behavior of small nanoparticles has attracted widespread attention in recent years, including aggregation-induced optical property changes and their applications, the effects of aggregation on biocompatibility and toxicity, and the shaping of nanocluster supracrystals by controlling the aggregation process.[16–19] Agglomeration-induced emission (AIE) of fluorescent metal nanoclusters, usually triggered by inorganic ions or special solvents, is becoming an important research focus,[20–22] and the reversible AIE of the nanoclusters has drawn the interest of

[1]Key Laboratory of Luminescent and Real-Time Analytical Chemistry (Southwest University), Ministry of Education, School of Chemistry and Chemical Engineering, Southwest University, Chongqing, PR China; [2]College of Chemistry and Pharmaceutical Engineering, Sichuan Provincial Academician (Expert) Workstation, Key Laboratory of Green Catalysis of Higher Education Institutes of Sichuan, Sichuan University of Science and Engineering, Zigong, PR China; [3]Chongqing Institute of Green and Intelligent Technology, Chinese Academy of Sciences, Chongqing, PR China and [4]School of Chemistry and Chemical Engineering, Chongqing University, Chongqing, PR China
Correspondence: Professor NB Li or Professor HQ Luo, Key Laboratory of Luminescent and Real-Time Analytical Chemistry (Southwest University), Ministry of Education, School of Chemistry and Chemical Engineering, Southwest University, Chongqing 400715, PR China.
E-mail: linb@swu.edu.cn or luohq@swu.edu.cn
Received 3 June 2016; revised 9 September 2016; accepted 27 September 2016

researchers.[23] In the published research, Au and Ag NCs that possess AIE are always stabilized by thiols, and recent studies show that the AIE effect of nanoclusters may be caused by the interaction between the metal core and ligands. The thiolate ligands and metal(I)−thiolate complexes coating the metal core are responsible for the AIE effect of metal nanoclusters.[8,24] Unlike AIE, the aggregation-induced quenching (AIQ) phenomenon of fluorescent nanoclusters has been studied and used to establish various sensors. However, to the best of our knowledge, most works reporting on the AIQ of fluorescent nanoclusters show that it is unidirectional and irreversible, and only a few have reported on the reversible agglomeration-induced quenching (R-AIQ) phenomenon of fluorescent metal nanoclusters. For example, Chen *et al.*[25] and Chang *et al.*[26] demonstrated the Cu^{2+}- and Hg^{2+}-induced R-AIQ of thiol-stabilized fluorescent Au nanoclusters. These agglomerations could be broken, and the nanoclusters could be redispersed by the addition of corresponding chelators, ethylenediaminetetraacetate for Cu^{2+} and biothiols for Hg^{2+}. García-Bosch *et al.*[27] reported that Ag NCs coated with multi-amino polymers showed R-AIQ by switching the temperature between 4 and 60 °C; moreover, the Ag NCs showed pH-induced aggregation, but aggregation caused by pH change is irreversible. Wang *et al.*[28] reported a reversible pH sensor based on fluorescent Cu nanoclusters and attributed the fluorescence quenching of the Cu nanoclusters to reversible agglomeration; unfortunately, the sensing mechanism used in that study is simple speculation and has not been further confirmed or discussed in detail. Accordingly, the study of the R-AIQ of fluorescent metal nanoclusters has not been explored in detail.

Herein, we report a simple etching method to obtain water-soluble fluorescent Ag NCs at room temperature, with citrate as the Ag nanocrystal stabilizer and GSH as the etchant to trigger the etching process from nanocrystals to nanoclusters; high-resolution transmission electron microscopy (HRTEM) images clearly recorded the nanoparticle transformation process. Moreover, we unexpectedly found that the prepared Ag NCs are very sensitive to the pH of solutions and possess pH-switchable agglomeration and dispersion behavior, accompanied by reversible changes in the fluorescence intensity and absorbance of the Ag NCs solution. However, the previously reported GSH-stabilized Ag NCs are less sensitive to changing pH in aqueous solution[29] and, to the best of our knowledge, the pH-switchable signal response of GSH-stabilized Ag NCs has not been reported. Furthermore, the distinctive pH-dependent R-AIQ behavior of the prepared Ag NCs was ascribed to the interaction between the amido functional groups of the ligands (GSH) and the carboxyl groups of citrate attached to the surface of the nanoclusters. The interesting R-AIQ behavior and the subtle effect of the functional groups on the Ag NCs surface provide a new perspective for investigating the physicochemical properties of ultrasmall metal nanoparticles in aqueous solutions. Moreover, the pH-switchable optical signal response offered a foundation for establishing regenerated sensors based on the prepared Ag NCs by changing the pH of solutions. In addition, to validate the practicability of the interesting pH-dependent R-AIQ phenomenon of the Ag NCs in the sensor field, we established urea and glucose sensors as an extended application study of the Ag NCs. According to reports that urea and glucose can change the pH of a solution by producing NH_3 and gluconic acid in the presence of urase and glucose oxidase (GOD),[30,31] we used the prepared Ag NCs as an optical probe to establish a regenerated sensing platform for detecting urea and glucose (Glu) in one sample, and the results were satisfactory.

MATERIALS AND METHODS

Chemicals and apparatus

Silver nitrate ($AgNO_3$), trisodium citrate dehydrate ($Na_3Cit{\bullet}2H_2O$), L-glutathione (GSH), sodium borohydride ($NaBH_4$), glucose (Glu) and urea were obtained from Aladdin Reagent Co. Ltd. (Shanghai, China). GOD and urease were obtained from Sangon Inc. (Shanghai, China). All reagents were analytical reagent grade, and all solutions were freshly prepared before use. Ultrapure water (18.2 MΩ cm) was used throughout the experiments.

The fluorescence and ultraviolet–visible (UV − vis) absorption spectra measurements were conducted using an F-2700 fluorescence spectrophotometer (Hitachi, Japan) and a UV-2450 spectrophotometer (Shimadzu, Japan), respectively. The slit widths were 10/10 nm for excitation and emission, and a photomultiplier tube voltage of 400 V was used for the fluorescence measurements. The HRTEM images were obtained using a Tecnai G2 F20 field emission transmission electron microscope (FEI, USA). Zeta potentials were measured by laser Doppler electrophoresis using a Zetasizer Nano ZS (Malvern Instruments Ltd, Malvern, UK). The pH of solutions was measured using a pH meter (PHS-3C, Shanghai Leici Instrument Company, Ltd, Shanghai, China). The Fourier transform infrared (FT-IR) spectra were measured using a Bruker IFS (Karlsruhe, Germany) 113v spectrometer after pelleting the fine powder with KBr; the Ag NCs sample was prepared by dialyzing for 12 h using a cellulose ester dialysis membrane with a molecular weight cutoff of 500 and removal of all water through a freeze-drying process.

Preparation of the fluorescent Ag nanoclusters

Typically, 200 μl of 100 mM Na_3Cit and 100 μl of 100 mM $AgNO_3$ solutions were first added to ultrapure water (1300 μl) under stirring for 3 min using Teflon-coated magnetic stirring bars, and then 15 μl of 20 mM $NaBH_4$ solution was slowly added to the solution under vigorous stirring, and the mixture was stirred for 30 min to ensure that an adequate reaction occurred. Subsequently, 150 μl of 200 mM GSH was added, and the solution was stirred for 10 min. The final solution was stored at room temperature (~25 °C) for at least 168 h before further use. Without any centrifugation or purification, an aqueous solution of 100-fold diluted Ag NCs was used as the optical probe to establish the sensing platform for urea and glucose.

pH response of the prepared Ag nanoclusters

The pH of the diluted 100-fold Ag NCs aqueous solution was measured using a pH meter and then solutions were adjusted to various pH values using 0.1 M NaOH and 0.1 M HNO_3 solutions. The Ag NCs solutions with various pH values were incubated for 40 min at room temperature before subjecting to fluorescence and UV − vis absorption spectra measurements.

Detection of urea and glucose

For the detection of urea, a urea solution (56 mM) was mixed with an equal volume of 10 mg ml^{-1} aqueous urease solution, and the mixture was incubated at 37 °C for 5 min. Subsequently, 10 μl of Ag NCs, water and various volumes of the above solutions were added, in order, to a 1.5 ml plastic centrifuge tube, and the total volume of the mixtures was maintained at 1 ml. The mixtures were stirred for ~1 min and incubated for 40 min at room temperature. Finally, the fluorescence and UV − vis absorption spectra of the above solutions were recorded in the 370–525 nm and 200 − 450 nm wavelength ranges, respectively.

For the detection of Glu, 56 mM urea and 500 mM Glu solution were mixed with equal volumes of 10 mg ml^{-1} urease and 20 mg ml^{-1} GOD in aqueous solution. The two mixtures were incubated at 37 °C for 5 and 20 min, respectively. Subsequently, 10 μl of Ag NCs, water, 6 μl of urea and urease solution, and various volumes of solutions containing Glu and GOD were added, in order, to a 1.5 ml plastic centrifuge tube, and the total volume of the mixtures was maintained at 1 ml. The mixtures were stirred for ~1 min and incubated for 40 min at room temperature before being subjected to fluorescence and UV − vis absorption spectra measurements.

RESULTS AND DISCUSSION

Synthesis and characterization of the fluorescent Ag nanoclusters

A simple etching method was used to obtain fluorescent Ag NCs from citrate-stabilized Ag nanocrystals at room temperature. Figure 1a shows the schematic of the synthesis route. The citrate had the role of stabilizer to protect the prepared Ag nanocrystals from aggregation and precipitation, and the GSH was used as an etchant to obtain fluorescent Ag NCs. The prepared Ag NCs were characterized using fluorescence and UV − vis spectrophotometry and HRTEM. Figure 1b shows that the maximum fluorescence excitation and emission wavelengths of the prepared Ag NCs were 348 and 428 nm, respectively; the diluted Ag NCs solution was colorless under visible light and emitted blue fluorescence under 365 nm UV light (inset in Figure 1b). Moreover, a sharp absorption peak at 349 nm and a shoulder peak at ~270 nm were observed in the UV–vis absorption spectrum. The optical properties of the Ag NCs were very similar to those of the reported GSH-templated Ag NCs.[32,33] In Figure 1c, the HRTEM image of the prepared Ag NCs shows that the Ag NCs were well-dispersed and uniform in the solution and that the average size was ~2 nm (inset in Figure 1c). The fluorescence quantum yield of the Ag NCs was ~1.8% in aqueous solution according to an established procedure[34] using the quinine sulfate as the reference. In addition, the bonding interaction between Ag NCs and GSH was confirmed by the FT-IR spectra and the energy dispersive X-ray spectrum. Supplementary Figure S1 in the Supporting Information shows that the S–H stretching band of GSH near 2524 cm^{-1} disappeared in the FT-IR spectrum of the Ag NCs, indicating the formation of a S–Ag covalent bond because of the thiol-Ag atom interaction. Moreover, the characteristic peaks of S (at ~2.30 keV) and Ag (at ~3.00 and 22.10 keV) could be observed from the energy dispersive X-ray spectrum of the Ag NCs, as shown in Supplementary Figure S2, which further verified that the S and Ag atoms existed in the ultrasmall nanoparticles.[33] Furthermore, we explored the stability of the prepared Ag NCs by monitoring the change of fluorescence intensity of the Ag NCs solution over time. Supplementary Figure S3 shows that the Ag NCs solution can maintain ~90% of its fluorescence intensity even after 90 days, showing that the prepared Ag NCs are stable for at least 3 months. Moreover, we tested the repeatability of the proposed synthesis method in this work using fluorescence and UV–vis absorption spectra measurements. Supplementary Figure S4a and b shows the results of fluorescence measurements ($\lambda_{ex} = 348$ nm, $\lambda_{em} = 428$ nm) for 10 prepared Ag NCs sample solutions obtained using the proposed synthesis method with their corresponding UV–vis absorption spectra, indicating that the 10 Ag NCs samples possessed identical optical properties. Moreover, the relative s.d. of the 10 fluorescence and absorbance ($\lambda = 349$ nm) measurements were 4.37 % and 4.94 %, respectively, demonstrating that the proposed synthesis method has good repeatability.

In addition, the entire etching process, from Ag nanocrystals to small nanoclusters, was monitored with HRTEM. Figure 2 clearly reveals the state transition of the Ag nanoparticles before (Figure 2a) and after GSH was added to the solutions (24, 72, 120 and 168 h in Figure 2b,c,e and f, respectively) at room temperature, indicating that the Ag nanoparticles stabilized with citrate existed in larger nanocrystals (Figure 2a), a few small-scale Ag nanoparticles were freed from the nanocrystals 24 h after the addition of GSH (Figure 2b), and all the nanocrystals were transformed into small nanoclusters after 168 h (Figure 2f). Figure 2d is an enlarged HRTEM image of a randomly selected Ag nanocrystal 72 h after GSH was added (Figure 2c). The fast Fourier transform patterns of Figure 2g and h show that the Ag nanocrystals in the etching process maintained a good lattice, corresponding to metallic silver, whereas the small nanoclusters failed to possess a metallic crystal lattice because of the quantum size effect (insets in Figure 2d and f).[3] The loss of the lattice was accompanied by the appearance of the size-dependent physicochemical properties of

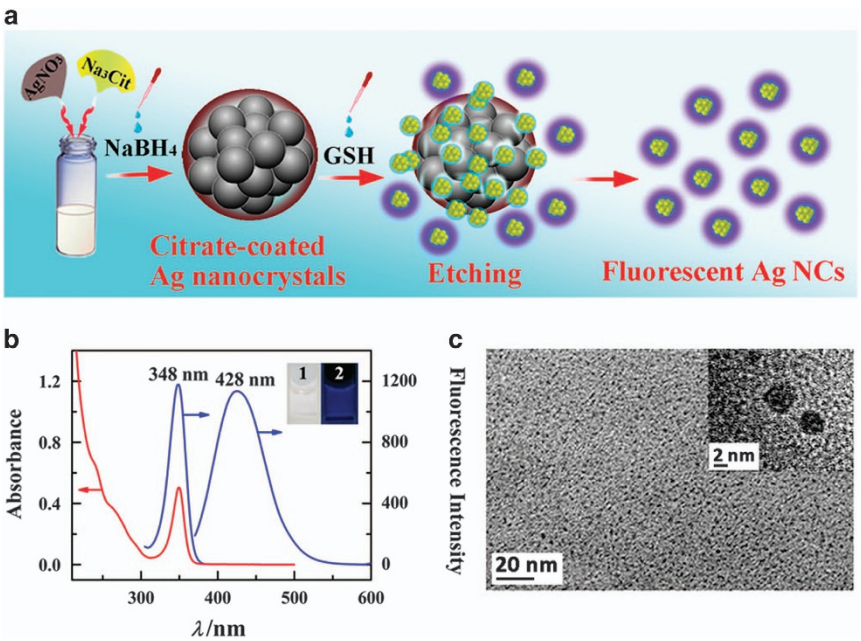

Figure 1 (**a**) Schematic of the route of Ag nanoclusters (Ag NCs) synthesis. (**b**) Fluorescence and ultraviolet–visible (UV–vis) absorption spectra of the diluted Ag NCs; the inset shows photographs of the diluted aqueous Ag NCs solutions under visible light (1) and UV light (2). (**c**) high-resolution transmission electron microscopy (HRTEM) image of the prepared Ag NCs (scale is 20 nm); the inset shows the magnified Ag NCs particles (scale is 2 nm).

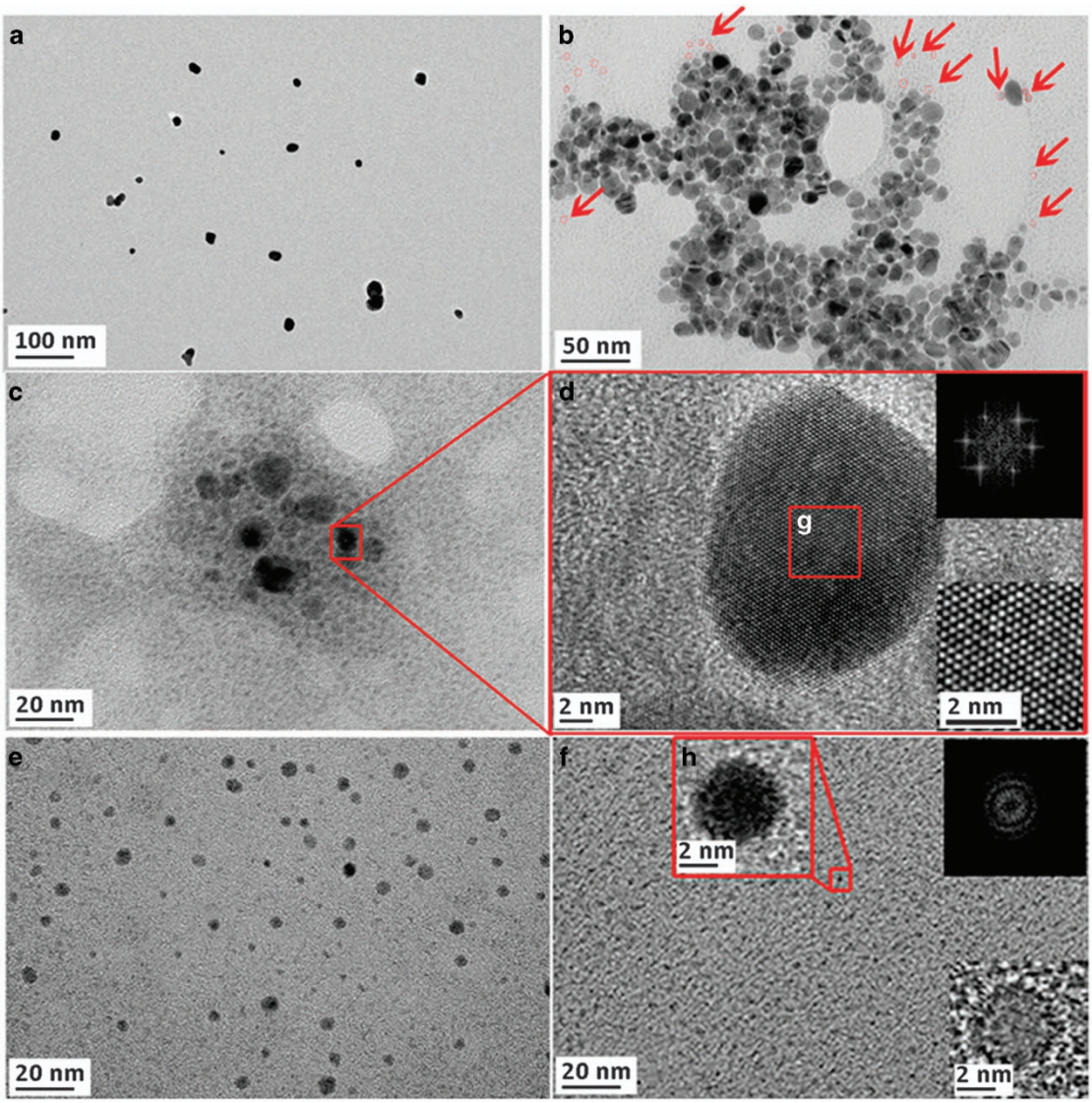

Figure 2 High-resolution transmission electron microscopy (HRTEM) images of Ag nanoparticles in the etching process before (**a**) and after the addition of GSH to the solution at 24 h (**b**), 72 h (**c**), 120 h (**e**), and 168 h (**f**); (**d**) is an enlarged image of a randomly selected Ag nanocrystal in **c**; the insets show the fast Fourier transform (FFT) patterns (up) and the corresponding inverse FFT patterns (down) of **g**, **h**.

the Ag NCs. Figure 3a and b describes the changes in the fluorescence and UV–vis absorption spectra during the etching process, showing that the fluorescence intensity at 428 nm and absorbance at 349 nm increased synchronously, and an obvious blue shift was observed at the UV–vis absorption peak within 12 h after the addition of GSH, which showed that the nanoparticles in the solution changed from larger nanocrystals to small nanoclusters, and the increasing absorbance showed the increase in the concentration of Ag NCs as the etching process progressed.[35,36] The color of the Ag colloid solution changed from the original dark brown (before adding GSH) to reddish-brown (72 h after the addition of GSH) and then to colorless after 168 h (Figure 3c), and the blue emission of the diluted Ag NCs solutions brightened correspondingly over time (Figure 3d).

Furthermore, we explored if the citrate is still present on the surface of Ag NCs after thiol etching using element analysis of the carbon (C) and sulfur (S) in the unpurified and purified Ag NCs samples. The purified Ag NCs were obtained by centrifugation (rotation speed: 13 000 r min^{-1}, 60 min) followed by dialysis (molecular weight cut-off: 1 KD, 24 h) of the prepared Ag NCs. The reaction reagents involved in this synthesis system are $AgNO_3$, $NaBH_4$, GSH and citrate. Among them, only GSH and citrate contain C and only GSH contains S, and the relative atomic masses of C and S are 12.01 and 32.07, respectively. Therefore, the ratio of the mass of C to S in GSH should be 3.745, and the molar ratio of GSH to citrate in this system is 3:2, so the mass ratio of C and S is 5.243. If the citrate involved is all present on the surface of the Ag NCs after thiol etching, the C/S mass ratio in the purified Ag NCs sample should still be 5.243; if a portion of the citrate is present on the surface of the Ag NCs after thiol etching, the C/S mass ratio in the purified Ag NCs sample should be <5.243 and >3.745; otherwise, the mass ratio of C and S in the purified Ag NCs sample will be maintained at 3.745 if citrate is not present on the surface of the Ag NCs after thiol etching. Accordingly, we can determine whether the citrate is still present on the surface of the Ag NCs after thiol etching by detecting the contents of C and S in the purified Ag NCs. The results of element analysis of C and S in the Ag NCs are listed in Table 1, showing that the C/S mass ratio in

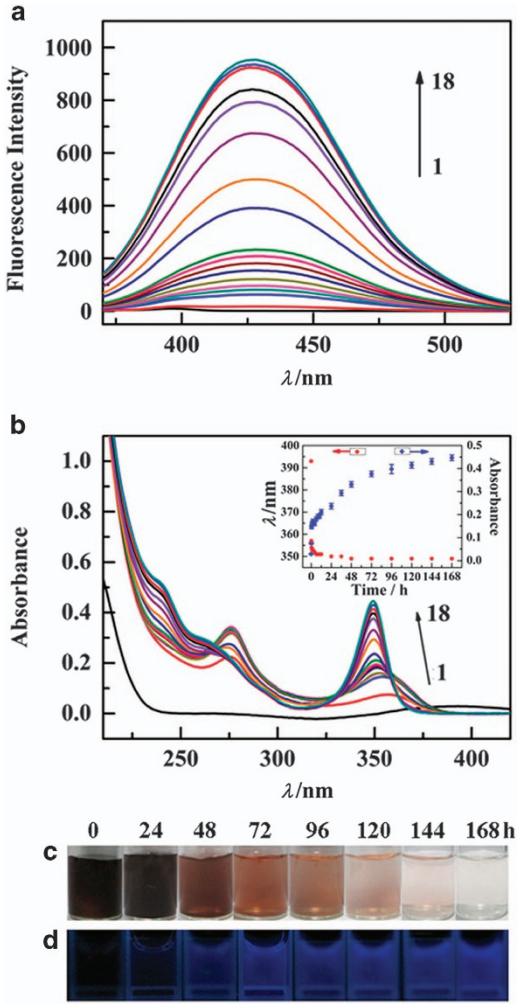

Figure 3 Time evolution of fluorescence (**a**) and ultraviolet–visible (UV – vis) absorption spectra (**b**) before (curve 1) and after the addition of GSH (curves 2–18: 0.5, 1, 1.5, 2, 4, 6, 8, 10, 12, 24, 36, 48, 72, 96, 120, 144 and 168 h). Photographs of original (**c**) and 100-fold diluted (**d**) aqueous Ag nanoclusters (Ag NCs) solutions for recording color changes over time under visible light (**c**) and UV light (**d**).

Table 1 Results of element analysis of C and S in Ag NCs

Sample	C *(%)*	S *(%)*	C/S *ratio*
Unpurified Ag NCs	27.27	5.182	5.262
Purified Ag NCs	27.11	7.256	3.736

Abbreviation: Ag NCs, Ag nanoclusters.
Note: the results represent mass percentages of the corresponding element in samples.

unpurified Ag NCs is 5.262 (error of ~1.9 %), which is consistent with the C/S ratio when all the GSH and citrate involved in the synthesis exist in the sample. The detected C/S mass ratio in the purified Ag NCs is 3.736, consistent with the C/S mass ratio in GSH (error of ~0.9 %). Therefore, the citrate is not present on the surface of the Ag NCs after thiol etching.

pH-dependent signal switching of the Ag nanoclusters

In this work, we were surprised to find that the fluorescence of the prepared Ag NCs is very sensitive to the pH of solutions, and the fluorescence intensity and absorbance of the Ag NCs solution decrease with increasing pH. Additional experiments showed that the fluorescence intensity and absorbance of the Ag NCs remained stable after a reaction time of 40 min in solutions of different pH (pH 5, 6, and 7; Supplementary Figure S5 in the Supporting Information). Figure 4a and b show that there was fairly good linearity between the fluorescence intensity at 428 nm and the pH of the solutions in the pH range of 5–7 after a reaction time of 40 min under the experimental conditions. The absorbance of the characteristic UV–vis absorption peak of the Ag NCs at 349 nm decreased in correspondence with increasing pH and maintained a linear relationship within pH 5 – 7 (Supplementary Figure S6a and b in the Supporting Information). Moreover, the additional studies indicated that the loss of fluorescence clearly recovered when the pH of the solution was again reduced to 5 (Figure 4c), and the change in absorbance of the Ag NCs was consistent with that of the fluorescence intensity (Supplementary Figure S7 in the Supporting Information). In addition, the fluorescence signal could be reversibly switched more than one time when the pH alternated between 5 and 7 (Figure 4d), and the pH-switchable signal response of the prepared Ag NCs had good repeatability under the experimental conditions, as shown in Supplementary Figure S8. Accordingly, quenching and recovery of the fluorescence (that is, turn off/on) can be achieved by adjusting the pH of the solution.

To investigate the mechanism of the pH-dependent signal switching of the fluorescent Ag NCs, the HRTEM technique was used to obtain HRTEM images of the Ag NCs at different stages in one cycle of this reversible behavior. The original Ag NCs (pH 5) dispersed well in the solution (Figure 4e), and the Ag NCs gathered (Figure 4f) when the pH of the solution was adjusted to 7 by adding 0.1 M NaOH and incubated for 40 min at room temperature, whereas the Ag NCs would redisperse well in the solution (Figure 4g) when the pH was first adjusted to 7 and then to 5 again with 0.1 M NaOH and HNO_3. The HRTEM results showed that under the experimental conditions, the Ag NCs possess the capability of reversible agglomeration and dispersion in aqueous solution with the change in pH.

The stability of a colloidal solution can be characterized by the Zeta (ξ) potential of the solution.[37] When the absolute value of ξ is >30 mV, the colloidal solution has good stability, and the nanoparticles can disperse well. When the absolute value of ξ is between 30 and 10 mV, the colloidal solution will become unstable, and the nanoparticles gradually begin to gather. When the absolute value of ξ is <5 mV, the solution will be highly unstable, and the colloidal particles will gather quickly. Therefore, the measurement of ξ potential was selected to further verify the reversible behavior of the Ag NCs in aqueous solution. The results showed that the ξ potential of the Ag NCs solution changed with the change of pH; when the pH of the solution was changed from 5 to 7 and then to 5 again, the ξ potential changed correspondingly from -39.6 to -15.8 mV and then to -38.1 mV, indicating that the Ag NCs solution had good stability when the pH was 5, that the solution became less stable and tended to agglomerate when the pH was adjusted to 7, and that the stability of the solution could be recovered by adjusting the pH to 5 again. Furthermore, the ξ potential was determined using phase analysis light scattering technology, as the phase plot records the phase difference of the particles between scattered light and reference light during the ξ potential test. For the stable colloidal solution, the phase plot has a good slope; we can clearly observe the phase transformation caused by the voltage transformation in the area of fast field reversal (FFR), and the curve presents a clear slope and good linearity in area of slow field reversal (SFR). Figure 4h–j shows the corresponding phase plots of the Ag NCs solution at different stages, illustrating that the Ag NCs

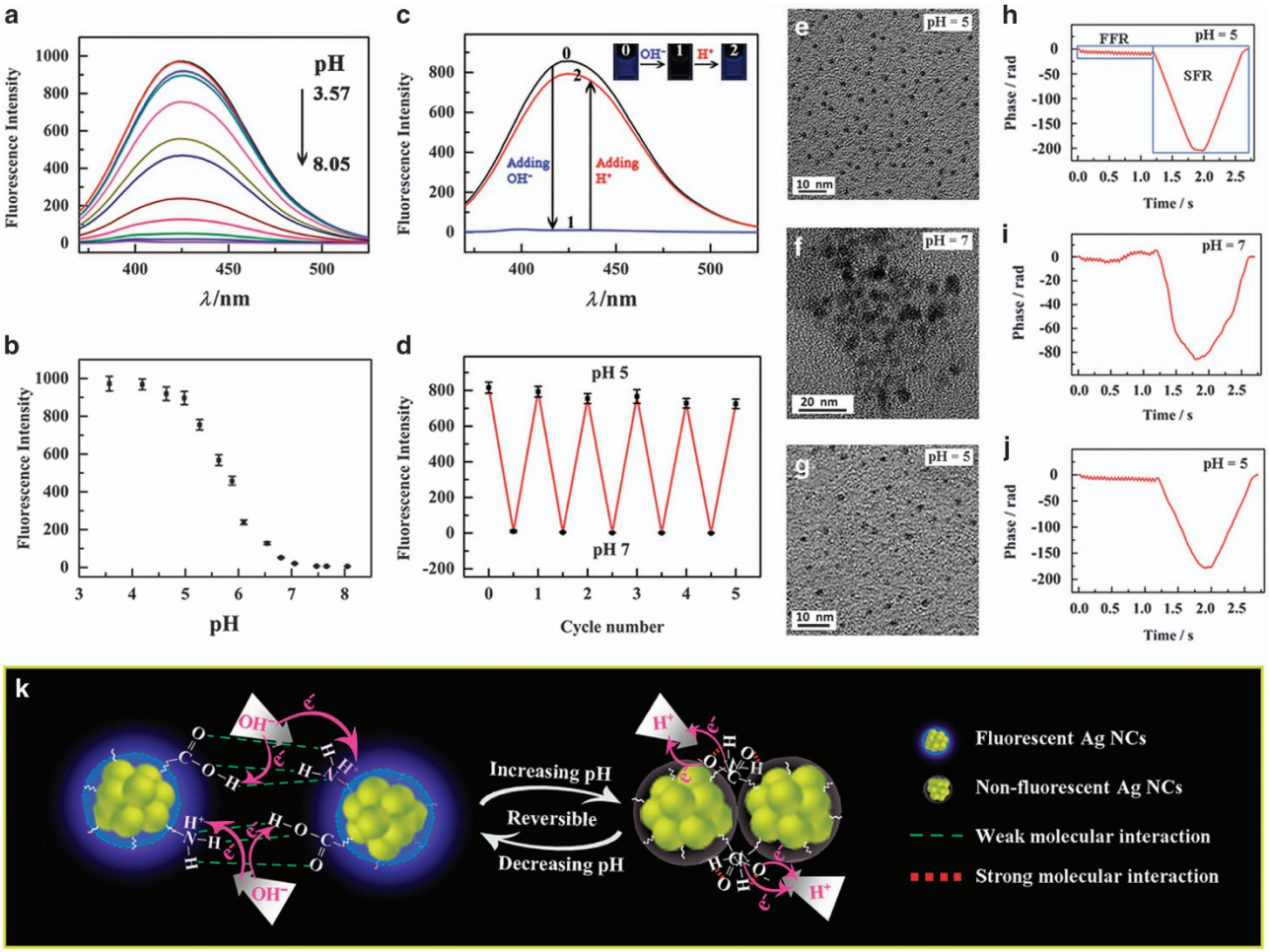

Figure 4 (**a**) Fluorescence spectra of the Ag nanoclusters (Ag NCs) in aqueous solutions of various pH (3.57, 4.19, 4.64, 4.98, 5.27, 5.88, 6.10, 6.54, 6.80, 7.06, 7.47, 7.66 and 8.05). (**b**) Plot of the fluorescence intensity of Ag NCs at 428 nm versus pH. (**c**) Fluorescence spectra of the original Ag NCs solution (curve 0, pH 5), the Ag NCs solution with pH adjusted to 7 by adding 0.1 M NaOH (curve 1) and the Ag NCs solution with pH adjusted to 7 and then to 5 with 0.1 M NaOH and HNO_3 solutions (curve 2); the inset shows the corresponding photographs under ultraviolet (UV) light. (**d**) Reversibility of fluorescent switching of the Ag NCs solution when the pH changes from 5 to 7. (**e**, **f**, **g**) show HRTEM images of the original Ag NCs solution (pH 5), the Ag NCs solution with pH adjusted to 7, and the Ag NCs solution with pH adjusted to 7 and then to 5. (**h**, **i**, **j**) show the corresponding phase plots of the Ag NCs solution when the pH changes from 5 to 7 and then to 5 again. (**k**) Schematic of pH-switchable interaction mechanism among the Ag NCs.

solution had good stability when the pH was 5 (Figure 4h and j) and that the solution was less stable when the pH was adjusted to 7 (Figure 4i). Compared with the corresponding HRTEM images, the information obtained from the results had a certain uniformity. The two characterizations indicated that the uniformly dispersed Ag NCs became unstable when the pH of the solution was adjusted to 7 and that the Ag NCs would gradually agglomerate, whereas the Ag NCs solution could return to a stable state and the nanoclusters could redisperse well in the solution by returning the pH to 5.

In addition, the pH-induced interaction mechanism among Ag NCs was studied. The 'agglomeration' of nanoparticles is different from 'aggregation', according to the International Union of Pure and Applied Chemistry definition. Agglomeration is a case in which the dispersed particles in solution are held together by weak interactions, ultimately resulting in phase separation, and the entire process is reversible, whereas aggregation is defined as particles joining by strong bonding interactions among the colloidal particles, and the clustering is irreversible.[38] Accordingly, we deduced that the increasing pH induced an increase in the weak interactions (for example, the Van der Waals forces and hydrogen bonding) among the Ag NCs and that although there is no direct contact between the citrate and Ag atoms after thiol etching, the citrate had a significant role in determining the reversible agglomeration and dispersion behavior of the prepared Ag NCs. We found that the fluorescence intensity and absorbance of the purified Ag NCs solutions maintained good linear relationships with the pH in the range of pH 5–7 (Supplementary Figure S9) and decreased with increasing pH; the reaction time required was greatly reduced in the purified Ag NCs solutions compared with that of the unpurified Ag NCs at the same pH (pH 7). As shown in Supplementary Figure S10, the fluorescence intensity of the purified Ag NCs solution could be reduced to ~5% in 20 min, but the unpurified Ag NCs solution needed 40 min to achieve the same quenching effect. However, the purified Ag NCs had almost lost the ability to restore the optical signals through pH-dependent reversibility, as shown in Supplementary Figure S11a and b. Furthermore, the HRTEM images (Supplementary Figure S11c,d and e) show that the purified Ag NCs maintain even dispersal at pH 7 and that the size of the nanoclusters does not obviously change with the change of solution pH. According to the results above, we deduced that the pH response mechanism of the unpurified Ag NCs may be different from

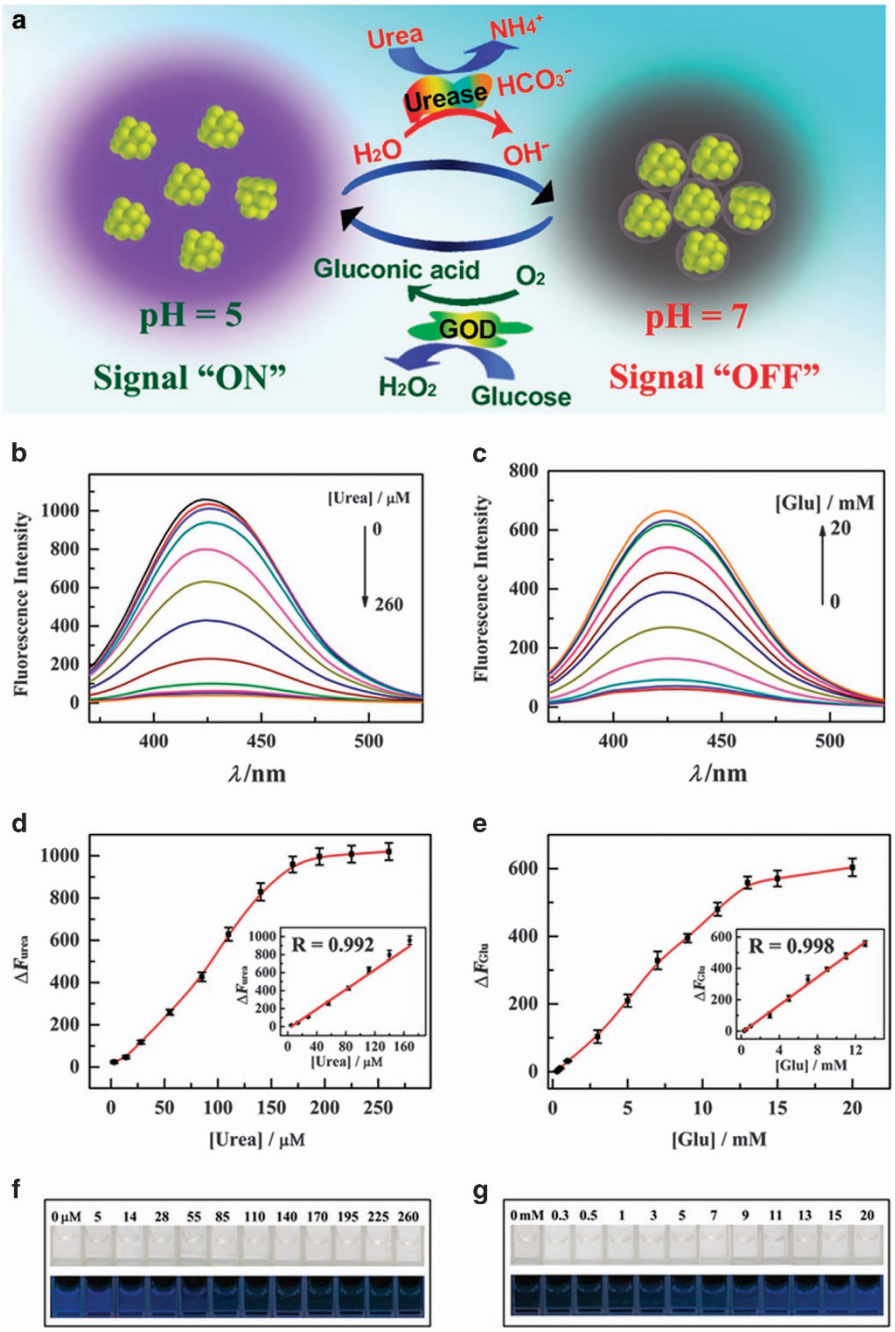

Figure 5 (**a**) Schematic sensing mechanism of the sensor for urea and Glu detection. (**b**) Fluorescence spectra of Ag NCs solutions containing various concentrations of urea (0, 5, 14, 28, 55, 85, 110, 140, 170, 195, 225 and 260 μM). (**c**) Fluorescence spectra of Ag NCs solutions containing 170 μM urea and various concentrations of Glu (0, 0.3, 0.5, 1, 3, 5, 7, 9, 11, 13, 15 and 20 mM). (**d**, **e**) show plots of the relative fluorescence intensity at 428 nm versus the concentrations of urea and Glu, respectively; the insets in **d**, **e** show the corresponding linear response regions for urea and Glu. (**f**, **g**) show photographs of the reaction solutions under visible light (top) and UV light (bottom) for urea and Glu detection, respectively.

that of the purified Ag NCs and that the citrate had a key role in the pH-switchable behavior of the Ag NCs. The citrate can attach to the Ag NCs surface by hydrogen bond interactions because the Ag NCs are rich in carboxyl groups after thiol etching. The carboxyl groups on the Ag NCs surface are similar to 'elastic cushions' and can reduce the impact caused by the pH change on Ag NCs, so the agglomeration among Ag NCs is slower in the presence of citrate in solution. The FT-IR spectrum of the Ag NCs supported this speculation (the red curve in Supplementary Figure S1). The peaks at ~3400, 3000 and 1520 cm^{-1} can be ascribed to the characteristic absorption bands of $-NH_2$. The peaks at ~1630 and 1410 cm^{-1} can be ascribed to the characteristic absorption bands of –COOH; in particular, the peaks at 1520 and 1410 cm^{-1} correspond to the flexural vibration modes of –NH in $-NH_2$ and –OH in –COOH,[39,40] respectively, indicating that the Ag NCs contain many $-NH_n$ ($n = 1$, 2) and –COOH functional groups and that hydrogen bonding must exist among the Ag NCs. The $-NH_n$ group is easily protonated to form an $-NH_{(n+1)}^+$ group in aqueous solution; when the pH of the solution

increases, the excess OH^- would neutralize the protons in $-NH_{(n+1)}^+$ and –COOH and cause an increase in the electron-donating ability of the N and C atoms, which enhanced the intermolecular interaction of hydrogen bonding among the Ag NCs and led to the agglomeration of Ag NCs. Conversely, the attachment of citrate to the Ag NCs surface made the distance between the Ag NCs metal centers longer and made the carboxyl groups of citrate on the Ag NCs surface lose contact with the metal centers; thus, the clustered small nanoparticles were not strong, and the weak interactions among Ag NCs were easily broken when the pH of the solution decreased, so the switchable agglomeration and dispersion of Ag NCs could be observed by reversibly changing the pH of the solution. Figure 4k illustrates the mechanism of the pH-switchable interaction among Ag NCs. However, the pH-dependent response mechanism of purified Ag NCs is not clear at present, and further exploration is necessary.

Combining the results above with the fluorescence and UV–vis absorption spectra in Supplementary Figure S7, we drew the conclusion that increasing the pH induced the agglomeration of Ag NCs by enhancing the intermolecular interaction of the nanoclusters, causing AIQ and a decrease in the characteristic absorption peak of fluorescent Ag NCs solutions, whereas when the pH was reduced, the fluorescence intensity and absorbance of the Ag NCs subsequently recovered. The introduction of citrate and GSH into the synthesis plays a very important role in the pH-switchable behavior of the Ag NCs, as the rich carboxyl and amino functional groups on citrate and GSH make the Ag NCs very sensitive to the pH of the solution. Thus, the prepared Ag NCs show R-AIQ behavior and a switchable signal response with changing solution pH.

Establishment of a urea and glucose sensor based on the pH-switchable performance of Ag nanoclusters

The practicality of the use of Ag NCs with R-AIQ in the sensor field was further explored as an extended application of the prepared Ag NCs. Urea and Glu can be catalyzed to produce NH_3 and gluconic acid using urease and GOD (Equations (1) and (2)), respectively, and the solution pH can be controlled by the concentrations of urea and Glu.[30,31] Because of the pH-induced switching behavior in fluorescence intensity and absorbance signals of the Ag NCs and the pH regulation function of urea and Glu in the enzyme-catalyzed reactions in solution, the prepared Ag NCs were developed as a switchable optical signal probe for urea and Glu detection based on analysis of fluorescence and UV–vis absorption spectra. Figure 5a shows the sensing mechanism of the sensor for urea and Glu detection.

$$NH_2CONH_2 + 3H_2O \xrightarrow{\text{urease}} 2NH_4^+ + HCO_3^- + OH^- \quad (1)$$

$$Glu + O_2 + H_2O \xrightarrow{GOD} \text{gluconic acid} + H_2O_2 \quad (2)$$

In this work, several factors that affect the sensing of urea and Glu are explored, including the probe concentration, incubation time of the target with the corresponding enzyme, and the reaction time of the sensing system. Both the signal strength and sensitivity of a sensor depend on the probe concentration. The fluorescence intensity of the probe will increase with its concentration within a certain range; fluorescence quenching is more efficient with a given quencher concentration, and the sensitivity is higher at a lower concentration of fluorescence probe,[41] so selecting an appropriate probe concentration is necessary for urea and Glu detection. Accordingly, Supplementary Figure S12 in the Supporting Information shows the relationship of the fluorescence intensity of the Ag NCs at 428 nm to different concentrations of the Ag NCs (Supplementary Figure S12a and b) and the concentration-dependent fluorescence quenching efficiency on the addition of urea (170 μM; Supplementary Figure S12c). The results showed that the concentration of 10 μl ml^{-1} Ag NCs was more conducive to the sensitive detection of urea, so it was chosen as the concentration for this sensing system. Subsequently, the urea/urease and Glu/GOD incubation times at 37 °C were investigated. Supplementary Figure S13 in the Supporting Information shows that the relative fluorescence intensity ($\Delta F_{urea} = F_0 - F_{urea}$) and pH could quickly reach steady state in the urea/urease reaction, and the incubation time had little effect on the hydrolysis of urea (Supplementary Figure S13a); in the Glu sensing system, the relative fluorescence intensity ($\Delta F_{Glu} = F_{Glu} - F_{urea}$) and pH of the solution reached steady state after 20 min of Glu/GOD incubation (Supplementary Figure S13b). F_0, F_{urea} and F_{Glu} represent the fluorescence intensity of the original Ag NCs solution, the solution containing Ag NCs and a certain amount of urea, and the solution containing Ag NCs, 170 μM urea and a certain amount of Glu, respectively. Incubation times of 5 and 20 min were selected to carry out the enzyme-catalyzed reaction of urea and Glu. Moreover, the optimal reaction times of the sensing system for urea and Glu were explored. Supplementary Figure S14 in the Supporting Information shows that the relative fluorescence intensity began to stabilize after 40 min for the detection of both urea and Glu and that the steady state could be maintained for at least 90 min; therefore, the 40 min reaction time was selected for both urea and Glu sensing.

Under the optimized conditions, the linearity and detection limit of this sensing system for urea and Glu detection were evaluated by varying the concentration of targets based on fluorescence and UV–vis absorption spectra analysis techniques. Figure 5b,d and f shows that the fluorescence intensity of the reaction solutions decreased with increasing urea concentration, and the relative fluorescence intensity (ΔF_{urea}) maintained a good linear correlation with the urea concentration in the range of 5 − 170 μM. The regression equation is $\Delta F_{urea} = 5.47\ C_{urea} - 26.22$ ($R = 0.992$), and the limit of detection (LOD) is 10 nM at a signal-to-noise ratio of 3. Figure 5c,e and g shows that the fluorescence intensity of the reaction solutions recovered with the addition of Glu and that there was a good linear relationship between the relative fluorescence intensity (ΔF_{Glua}) and the concentration of Glu in the range of 0.3–13 mM. The corresponding regression equation is $\Delta F_{Glu} = 44.54\ C_{Glu} - 11.96$ ($R = 0.998$), and the limit of detection is 10 μM at a signal-to-noise ratio of 3. Supplementary Figure S15 shows the similar linear response ranges of urea (Supplementary Figure S15a and c) and Glu (Supplementary Figure S15b and d) sensing based on UV–vis spectrophotometry.

In addition, the selectivity of the sensing system was investigated by testing the sensing signal response of possibly coexistent substances such as carbohydrates (including maltose (Mal), fructose (Fru), lactose (Lac), and saccharose (Sac)), uric acid (UA) and inorganic salts (including NaCl, $NaNO_3$ and KNO_3). The results are shown in Supplementary Figure S16 in the Supporting Information, indicating that these substances had little effect on urea and Glu detection, even at much higher concentrations than those of the targets (the concentrations of these substances were all 20 mM) except UA. The effect of UA was mainly attributed to the high acidity of the aqueous UA solution and because UA donates H^+, leading to a decrease in the pH of the reaction solution and interference in the detection of urea and Glu.[42] Moreover, the reversible pH-dependent signal response behavior of the Ag NCs is reproduced in the sensing system for urea and Glu detection. Figure 6a shows that the pH of the reaction system could alternate between 5 and 7 by adding urea and Glu to the solution and that the fluorescence signal turned on and off

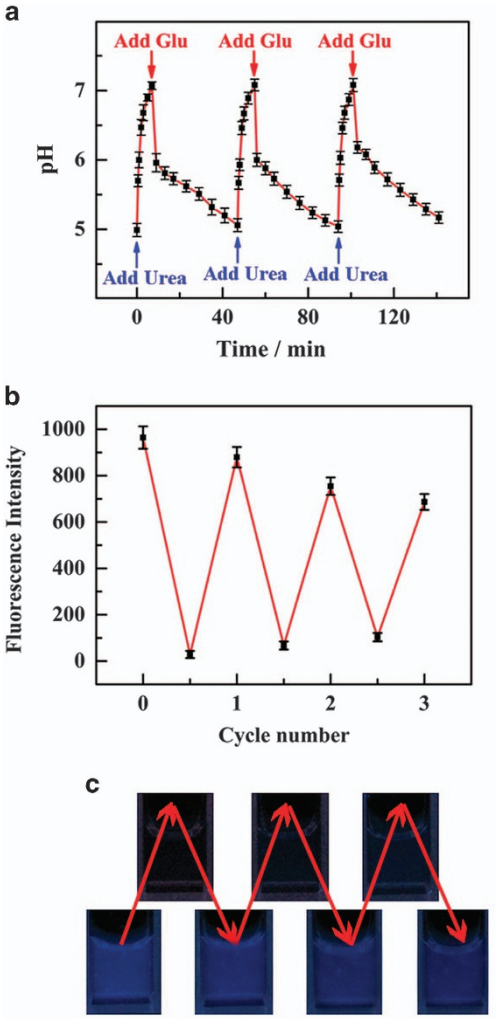

Figure 6 (**a**) Time-dependent pH change and (**b**) fluorescence intensity of the reaction system triggered by alternately adding urea and Glu to the solution. (**c**) Corresponding photographs under ultraviolet light.

with the change in pH (Figure 6b and c), indicating that this Ag NCs-based sensing system was regenerative for urea and Glu detection and that the regenerability of this sensor makes it more applicable and meaningful. We further explored the feasibility of this sensor for detecting urea and Glu in human serum and urine samples, and the results were satisfactory, as shown in Supplementary Tables S1 and S2.

CONCLUSIONS

In summary, we reported a facile etching method for generating water-soluble fluorescent Ag NCs with pH-switchable R-AIQ performance at room temperature. In this method, citrate-stabilized Ag nanocrystals were used as precursors, and GSH was the etchant. The entire etching process was monitored using HRTEM images, and the corresponding change in spectral properties during the size transformation was recorded by the fluorescence and UV − vis absorption spectra. Moreover, the pH-switchable signal response of the prepared Ag NCs was investigated in detail. Citrate and GSH have key roles in the pH-switchable behavior because of the rich carboxyl and amino groups of the ligands, and the pH-dependent reversible response is attributable to the pH-induced change in the electron-donating ability of the functional groups (including carboxyl and amino groups) on the Ag NCs, which further alter the hydrogen bonding among the Ag NCs, leading to their agglomeration or dispersion accompanied by the switch of fluorescence and UV − vis absorption peak signals. In addition, we further explored the practicality of Ag NCs in the sensor field based on their pH-switchable capability. The Ag NCs were developed as an optical probe to detect urea and Glu in a sample based on a target-triggered pH change of the solution by enzyme-catalyzed reactions, and the results were satisfactory. We hope that this work provides new insights to explore the effects of surface functional groups on the physicochemical properties of small nanoparticles in aqueous solutions and stimulates and encourages more theoretical and practical application studies on the R-AIQ of fluorescent metal nanoclusters.

CONFLICT OF INTEREST

The authors declare no conflicts of interest.

ACKNOWLEDGEMENTS

This work was financially supported by the National Natural Science Foundation of China (No 21273174, 21675131), the Municipal Science Foundation of Chongqing City (No CSTC-2013jjB00002, CSTC-2015jcyjB50001) and the Innovation Foundation of Chongqing City for Postgraduates (CYB2015059).

1 Zhang, Q., Xie, J., Yang, J. & Lee, J. Y. Monodisperse icosahedral Ag, Au, and Pd nanoparticles: Size control strategy and superlattice formation. *ACS Nano* **3**, 139–148 (2008).
2 Zheng, J., Nicovich, P. R. & Dickson, R. M. Highly fluorescent noble metal quantum dots. *Annu. Rev. Phys. Chem.* **58**, 409–431 (2007).
3 Qu, F., Li, N. B. & Luo, H. Q. Transition from nanoparticles to nanoclusters: microscopic and spectroscopic investigation of size-dependent physicochemical properties of polyamine-functionalized silver nanoclusters. *J. Phys. Chem. C* **117**, 3548–3555 (2013).
4 Wu, Z. & Jin, R. Transition from nanoparticles to nanoclusters: microscopic and spectroscopic investigation of size-dependent physicochemical properties of polyamine-punctionalized silver nanoclusters. *Nano Lett.* **10**, 2568–2573 (2010).
5 Zheng, K., Yuan, X., Kuah, K., Luo, Z., Yao, Q., Zhang, Q. & Xie, J. Boiling water synthesis of ultrastable thiolated silver nanoclusters with aggregation-induced emission. *Chem. Commun.* **51**, 15165–15168 (2015).
6 Qu, F., Li, N. B. & Luo, H. Q. Highly sensitive fluorescent and colorimetric ph sensor based on polyethylenimine-capped silver nanoclusters. *Langmuir* **29**, 1199–1205 (2013).
7 Ma, J. L., Yin, B. C., Le, H. N. & Ye, B. C. Label-free detection of sequence-specific dna based on fluorescent silver nanoclusters-assisted surface plasmon-enhanced energy transfer. *ACS Appl. Mater. Interfaces* **7**, 12856–12863 (2015).
8 Goswami, N., Yao, Q., Luo, Z., Li, J., Chen, T. & Xie, J. Luminescent metal nanoclusters with aggregation-induced emission. *J. Phys. Chem. Lett.* **7**, 962–975 (2016).
9 Song, X. R., Goswami, N., Yang, H. H. & Xie, J. Functionalization of metal nanoclusters for biomedical applications. *Analyst* **141**, 3126–3140 (2016).
10 Yao, Q., Yuan, X., Yu, Y., Yu, Y., Xie, J. & Lee, J. Y. Introducing amphiphilicity to noble metal nanoclusters via phase-transfer driven ion-pairing reaction. *J. Am. Chem. Soc.* **137**, 2128–2136 (2015).
11 Zheng, K., Yuan, X., Goswami, N., Zhang, Q. & Xie, J. Recent advances in the synthesis, characterization, and biomedical applications of ultrasmall thiolated silver nanoclusters. *RSC Adv.* **4**, 60581–60596 (2014).
12 Duan, H. & Nie, S. Etching colloidal gold nanocrystals with hyperbranched and multivalent polymers: A new route to fluorescent and water-soluble atomic clusters. *J. Am. Chem. Soc.* **129**, 2412–2413 (2007).
13 Balasubramanian, R., Guo, R., Mills, A. J. & Murray, R. W. Reaction of $Au_{55}(PPh_3)_{12}Cl_6$ with thiols yields thiolate monolayer protected Au_{75} clusters. *J. Am. Chem. Soc.* **127**, 8126–8132 (2005).
14 Qian, H., Zhu, Y. & Jin, R. Size-focusing synthesis, optical and electrochemical properties of monodisperse $Au_{38}(SC_2H_4Ph)_{24}$ nanoclusters. *ACS Nano* **3**, 3795–3803 (2009).
15 Muhammed, M. A. H., Aldeek, F., Palui, G., Trapiella-Alfonso, L. & Mattoussi, H. Growth of in situ functionalized luminescent silver nanoclusters by direct reduction and size focusing. *ACS Nano* **6**, 8950–8961 (2012).
16 Jeffrey, C. F. Simple and rapid colorimetric enzyme sensing assays using non-crosslinking gold nanoparticle aggregation. *Chem. Commun.* **36**, 3729–3731 (2007).
17 Díez, I., Pusa, M., Kulmala, S., Jiang, H., Walther, A., Goldmann, A. S., Müller, A. H. E., Ikkala, O. & Ras, R. H. Color tunability and electrochemiluminescence of silver nanoclusters. *Angew. Chem. Int. Ed.* **48**, 2122–2125 (2009).

18 Albanese, A. & Chan, W. C. Effect of gold nanoparticle aggregation on cell uptake and toxicity. *ACS Nano* **5**, 5478–5489 (2011).
19 Yao, Q., Yu, Y., Yuan, X., Yu, Y., Zhao, D., Xie, J. & Lee, J. Y. Counterion-assisted shaping of nanocluster supracrystals. *Angew. Chem. Int. Ed.* **54**, 184–189 (2015).
20 Jia, X., Li, J. & Wang, E. Cu nanoclusters with aggregation induced emission enhancement. *Small* **9**, 3873–3879 (2013).
21 Dou, X., Yuan, X., Yu, Y., Luo, Z., Yao, Q., Leong, D. T. & Xie, J. Lighting up thiolated Au@Ag nanoclusters via aggregation-induced emission. *Nanoscale* **6**, 157–161 (2014).
22 Zhang, L., He, N. & Lu, C. Aggregation-induced emission: a simple strategy to improve chemiluminescence resonance energy transfer. *Anal. Chem.* **87**, 1351–1357 (2015).
23 Luo, Z., Yuan, X., Yu, Y., Zhang, Q., Leong, D. T., Lee, J. Y. & Xie, J. From aggregation-induced emission of Au(I) – thiolate complexes to ultrabright Au(0)@Au(I) – thiolate core – shell nanoclusters. *J. Am. Chem. Soc.* **134**, 16662–16670 (2012).
24 Yu, Y., Luo, Z., Chevrier, D. M., Leong, D. T., Zhang, P., Jiang, D. E. & Xie, J. Identification of a highly luminescent $Au_{22}(SG)_{18}$ nanocluster. *J. Am. Chem. Soc.* **136**, 1246–1249 (2014).
25 Chen, W., Tu, X. & Guo, X. Fluorescent gold nanoparticles-based fluorescence sensor for Cu^{2+} ions. *Chem. Commun.* **13**, 1736–1738 (2009).
26 Chang, H. C., Chang, Y. F., Fan, N. C. & Ho, J. A. A. Facile preparation of high-quantum-yield gold nanoclusters: application to probing mercuric ions and biothiols. *ACS Appl. Mater. Interfaces* **6**, 18824–18831 (2014).
27 García-Bosch, N., Liras, M., Quijada-Garrido, I. & García, O. Multiamino polymeric capping of fluorescent silver nanodots as an effective protective, amphiphilic and pH/thermo-responsive coating. *RSC Adv.* **6**, 67643–67650 (2016).
28 Wang, W., Leng, F., Zhan, L., Chang, Y., Yang, X. X., Lan, J. & Huang, C. Z. One-step prepared fluorescent copper nanoclusters for reversible ph-sensing. *Analyst* **139**, 2990–2993 (2014).
29 Chen, Z., Lu, D., Zhang, G., Yang, J., Dong, C. & Shuang, S. Glutathione capped silver nanoclusters-based fluorescent probe for highly sensitive detection of Fe^{3+}. *Sens. Actuators B Chem.* **202**, 631–637 (2014).
30 Tremey, E., Suraniti, E., Courjean, O., Gounel, S., Stines-Chaumeil, C., Louerat, F. & Mano, N. Switching an O_2 sensitive glucose oxidase bioelectrode into an almost insensitive one by cofactor redesign. *Chem. Commun.* **50**, 5912–5914 (2014).
31 Tam, T. K., Strack, G., Pita, M. & Katz, E. Biofuel cell logically controlled by antigen-antibody recognition: Towards immune-regulated bioelectronic devices. *J. Am. Chem. Soc.* **131**, 11670–11671 (2009).
32 Yuan, X., Yeow, T. J., Zhang, Q., Lee, J. Y. & Xie, J. Highly luminescent Ag^{+} nanoclusters for Hg^{2+} ion detection. *Nanoscale* **4**, 1968–1971 (2012).
33 Zhou, T., Rong, M., Cai, Z., Yang, C. J. & Chen, X. Sonochemical synthesis of highly fluorescent glutathione-stabilized Ag nanoclusters and S^{2-} sensing. *Nanoscale* **4**, 4103–4106 (2012).
34 Lu, W., Qin, X., Liu, S., Chang, G., Zhang, Y., Luo, Y., Asiri, A. M., Al-Youbi, A. O. & Sun, X. Economical, green synthesis of fluorescent carbon nanoparticles and their use as probes for sensitive and selective detection of mercury (II) ions. *Anal. Chem.* **84**, 5351–5357 (2012).
35 Dong, J. X., Qu, F., Li, N. B. & Luo, H. Q. Aggregation, dissolution and cyclic regeneration of Ag nanoclusters based on ph-induced conformational changes of polyethyleneimine template in aqueous solutions. *RSC Adv.* **5**, 6043–6050 (2015).
36 Qin, Y., Ji, X., Jing, J., Liu, H., Wu, H. & Yang, W. Size control over spherical silver nanoparticles by ascorbic acid reduction. *Colloid Surf. A* **372**, 172–176 (2010).
37 Freitas, C. & Müller, R. H. Effect of light and temperature on zeta potential and physical stability in solid lipid nanoparticle (SLN) dispersions. *Int. J. Phytoremdiat.* **168**, 221–229 (1998).
38 Sokolov, S. V., Tschulik, K., Batchelor-McAuley, C., Jurkschat, K. & Compton, R.G. Reversible or not? Distinguishing agglomeration and aggregation at the nanoscale. *Anal. Chem.* **87**, 10033–10039 (2015).
39 Silverstein, R. M., Webster, F. X. *Spectrometric Identification of Organic Compounds* 6th edn (eds Silverstein R. M. & Webster F. X.) (Wiley: New York, NY, USA, 1998).
40 Solomons, T. W. G., Fryhle, C. *Organic Chemistry* 7th edn (eds Solomons T. W. G. & Fryhle C.) (Wiley: New York, NY, USA, 2001).
41 Qu, F., Li, N. B. & Luo, H. Q. Polyethyleneimine-templated Ag nanoclusters: a new fluorescent and colorimetric platform for sensitive and selective sensing halide ions and high disturbance-tolerant recognitions of iodide and bromide in coexistence with chloride under condition of high ionic strength. *Anal. Chem.* **84**, 10373–10379 (2012).
42 Song, Y., Liu, H., Tan, H., Xu, F., Jia, J., Zhang, L., Zhuang, L. & Wang, L. pH-switchable electrochemical sensing platform based on chitosan reduced graphene oxide/concanavalin a layer for assay of glucose and urea. *Anal. Chem.* **86**, 1980–1987 (2014).

Supplementary Information accompanies the paper on the NPG Asia Materials website (http://www.nature.com/am)